



# Wear Behavior of ZTA Reinforced Iron Matrix Composites

Lei Fan<sup>1</sup>(✉), Huahui Chen<sup>1</sup>, Haicun Li<sup>1</sup>, Daoren Fu<sup>1</sup>,  
and Haiping Hong<sup>2</sup>

<sup>1</sup> China University of Mining and Technology (Beijing), Beijing 100083, China  
{109047, chh}@cumtb.edu.cn

<sup>2</sup> South Dakota School of Mines and Technology, Rapid, SD 57701, USA

**Abstract.** Zirconia toughened alumina particles (ZTA<sub>p</sub>), both spherical (s-ZTA<sub>p</sub>) and irregular (i-ZTA<sub>p</sub>), reinforced iron (Fe45) matrix composites were fabricated by vacuum sintering. The influence of ZTA<sub>p</sub> size, shape and content in the microstructure and properties was investigated as well. Sliding wear and three-body rubber wheel abrasive wear tests were conducted for the composites. For the sliding wear test, Al<sub>2</sub>O<sub>3</sub> wheel and 200 N load force were used and for the three-body wear test, abrasive was 0.2–0.4 mm quartz sand and feeding rate 350 g/min at 130 N load force. The microstructure, phase constituent, interface bonding and morphology were analyzed by X-ray diffraction (XRD), scanning electron microscope (SEM) and related energy-dispersive X-ray spectroscopy (EDS). The results show that phase constituent of the composites consists of Fe-Cr-Ni, (Fe, Cr)<sub>7</sub>C<sub>3</sub>, FeCrB, Al<sub>2</sub>O<sub>3</sub> and ZrO<sub>2</sub>, the interface bonding between the ZTA<sub>p</sub> and Fe45 matrix presents non-chemical bonding. The composite with 30 vol. % ZTA particles exhibits the best wear resistance during sliding wear test. The supportive effect of iron matrix on ZTA<sub>p</sub> and the protective effect of ZTA<sub>p</sub> on the iron matrix of the composite improve wear resistance of the composites during the three-body abrasive wear process. Comparing to s-ZTA<sub>p</sub>, i-ZTA<sub>p</sub> is not easy to be pulled off due to its higher hardness and more suitable shape, therefore, i-ZTA<sub>p</sub> reinforced iron matrix composites show better wear resistance during the wear process.

**Keywords:** ZTA · Iron · Composite · Sliding wear · Abrasive wear

## 1 Introduction

In recent years, particle reinforced metal matrix composites (PRMMCs) have been widely studied by scholars in the world [1–4]. The composites take the advantage of high hardness, strength and wear resistance of ceramic particles and that of high toughness of metals. Therefore, they will be potential materials for application to harsh abrasive wear conditions.

For excellent technical properties, alumina was used as engineering ceramics [5]. However, the critical drawback of alumina is its poor fracture toughness. In order to improve the fracture toughness of alumina, Maiti [6] has tried to add zirconia into alumina, defined as zirconia toughened alumina (ZTA). The main toughening

mechanisms of ZTA are phase transformation and micro-cracks toughening [7, 8]. The increase of toughness can also improve its wear resistance [9]. The research on particle reinforced metal matrix composites mainly concentrates to Al, Mg, Ni, Ti, Cu and Zn matrix [10–15], and a few research on Fe matrix [16]. Iron matrix composites have low cost, high hardness and good mechanical properties, therefore ZTA particles reinforced iron matrix composite will not only have good mechanical properties but also good wear resistance. Compared with foundry technology, powder metallurgy technology has net shaping, cleaning and green environment advantages, furthermore it can produce the composites with high volume particles fraction [17–19]. At present, it is difficult to find the literature on particle reinforced iron matrix composites prepared by powder metallurgy, as well as the research on wear behavior of the composites.

In this paper, ZTA particles reinforced iron matrix composites by powder metallurgy technology were fabricated, the effect of particle size, shape and content on wear behavior of the composites and their wear mechanism were studied and analyzed.

## 2 Experimental Details

### 2.1 Composites Preparation

The iron matrix powder is about 50  $\mu\text{m}$  Fe-based self-fluxing alloy powder (Fe45). The composition is shown in Table 1. Three kinds of ZTA particle size, spherical ZTA particles (s-ZTA) and irregular ZTA particles (i-ZTA), are used. Composition of i-ZTA particle is shown in Table 2. The microstructures of i-ZTA and s-ZTA are shown in Fig. 1.

**Table 1.** Chemical compositions and main properties of Fe-based self-fluxing alloy

	Contents (wt%)						Properties		
	C	B	Si	Cr	Fe	Ni	Density $\text{g/cm}^3$	Melting point/ $^{\circ}\text{C}$	Hardness/HRC
Fe 45	0.6–0.9	3–4	3–4	16–18	Others	12–14	7.56	1217	42–48

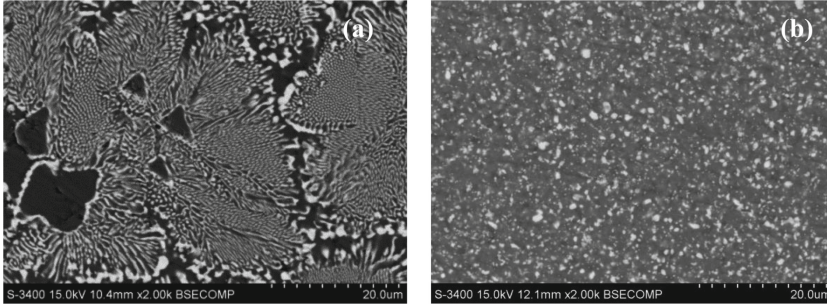
The components of composite specimens used for wear tests were designed and shown in Table 3. The sum of the volume fraction of the particles and the matrix is 100% (e.g., 20 vol. % F14 (2 mm) + 80 vol. % Fe45 = 100%).

The Fe45 matrix composites reinforced by ZTA<sub>p</sub> were sintered in vacuum and the processing procedure was listed as following:

The first step was to mix ingredients. The ZTA particles were cleaned by anhydrous ethanol solution, which can avoid the effect on structure and properties of composites by impurities after later sintering progress. ZTA<sub>p</sub> and Fe45 powder, with 3 wt% added forming agent, were fully blended about 120 s in high-speed pendulum ball mill so that the ZTA particles were wrapped up with the Fe45 powder.

**Table 2.** Chemical compositions of i-ZTA particles (wt%).

Al <sub>2</sub> O <sub>3</sub>	ZrO <sub>2</sub>	TiO <sub>2</sub>	CaO	SiO <sub>2</sub>	MgO	Fe <sub>2</sub> O <sub>3</sub>	Na <sub>2</sub> O
60	39	0.45	0.09	0.1	0.02	0.15	0.03

**Fig. 1.** Microstructure of ZTA (a) i-ZTA, (b) s-ZTA**Table 3.** Components of the composite specimens

Specimens no.	Components/vol. %		
	Particle/vol. %		Matrix/vol. %
F14/Fe45	i-ZTA	F14(2 mm)/(20/30/40/50) vol. %	Fe45/(80/70/60/50) vol. %
F30/Fe45			
F150/Fe45		F30(1 mm)/(20/30/40/50) vol. %	Fe45/(80/70/60/50) vol. %
s-ZTA/Fe45		F150(0.1 mm)/(20/30/40/50) vol. %	Fe45/(80/70/60/50) vol. %
Fe45	s-ZTA(2 mm)/(20/30/40/50) vol. %		Fe45/(80/70/60/50) vol. %
	None		100

The second step was to put the mixed powder into the mold and form the shaping by cold pressure process, keeping for 2 min at 15 t of pressure at first, then for 3 min at 24 t of pressure and at last for 5 min at 30 t of pressure.

The last step was to put the formed samples into the vacuum sintering furnace and heated at the heating rate of 10 °C/min, keeping for 15 min at 560 °C and 40 min at 1210 °C respectively. In order to avoid the micro-cracking of the composite samples the slow cooling with the furnace to room temperature was adopted.

The processing procedure described above is summarized in Fig. 2.

The phase constituents of the composites after sintered were analyzed by Rigaku D/max-2500PC X-ray diffraction (XRD) with Cu-K $\alpha$  ( $\lambda = 1.5406 \text{ \AA}$ ) radiation at an operating voltage of 40 kV and filament current of 40 mA. The diffraction angle ( $2\theta$ ) at which the X-rays hit the sample varied from 20° to 90° with a step size of 0.05° and testing time of 1 s in each step.

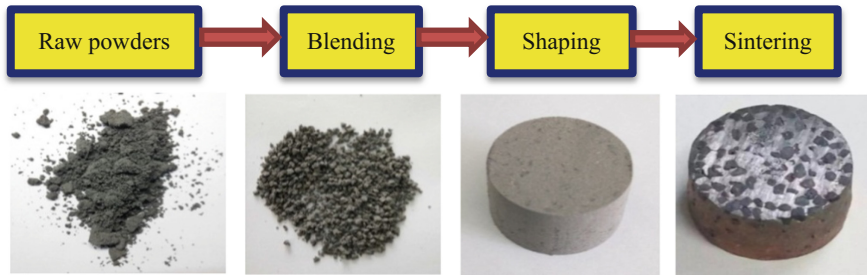


**Fig. 2.** Fabrication process of ZTA reinforced iron matrix composite specimens

Microstructure of the composites and interface between ZTA and iron matrix were examined by Hitachi S-3400 N scanning electron microscopy (SEM). Elemental compositions and distributions were determined by energy dispersive OXFORD X-ray spectroscopy (EDS). To achieve a better resolution on the SEM images, each sample was sputter-coated with an ultrathin film of gold before the observation.

The density of composites was measured by the drainage method according to the Archimedes principle and hardness of the composite specimens was measured by HBRVU-187.5 briny optical hardness tester.

## 2.2 Sliding Wear Test

The sliding wear test of ZTA reinforced iron matrix composites was conducted by M-200 ring block wear tester with  $\text{Al}_2\text{O}_3$  wheel that has hardness about 1600 HV. The test samples were grounded and polished to ensure surface roughness and uniform. The rotational speed of the grinding wheel was 240 r/min, the load force was 200 N, and the wear time was 30 min. In order to ensure that the wear tests of different samples are under the same conditions, the grinding wheel was polished by 200, 400, 600, 800, and 1000 sandpaper before each wear test, so as to ensure the same roughness of the grinding wheel used for each wear test. Three samples were tested for each experiment condition. A schematic diagram of sliding wear test is shown in Fig. 3. The sample size is 12 mm  $\times$  10 mm  $\times$  10 mm.

After the wear test, ultrasonic cleaning using anhydrous ethanol solution and vacuum drying were performed for the samples. The mass loss of the sample before and after wear was measured by the XEL200 electronic balance with a precision of 0.0001 g. The wear volume was calculated to evaluate wear resistance of the composites. The morphology of worn samples was observed by SEM and the mechanism was discussed.

## 2.3 Three-Body Abrasive Wear Test

Three-body abrasive wear test for the composites was conducted with MLG-130 rubber wheel abrasive wear tester. The rubber wheel rotated at  $200 \pm 10$  r/min under 130 N load force for 10 min. The hardness of the rubber wheel was about HA 60 and the abrasive was 0.2–0.4 mm quartz sand with feeding of 350 g/min. Figure 4(a) shows

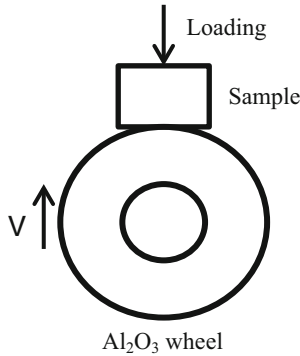


Fig. 3. Schematic diagram of sliding wear test

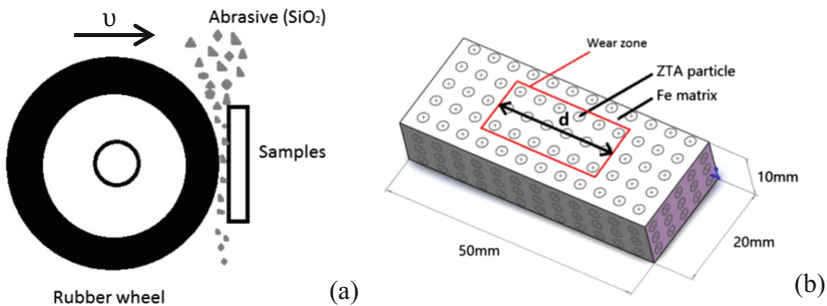


Fig. 4. Schematic diagram of the three-body abrasive wear test (a) and sample (b).

the schematic diagram of the three-body abrasive wear test and sample size is 50 mm × 20 mm × 10 mm as Fig. 4(b).

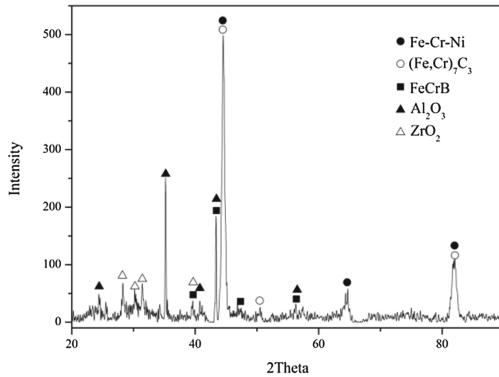
In order to compare the wear resistance of the composites, the three-body abrasive wear test of the Fe45 matrix samples without ZTA particles was also conducted.

Worn length *d* (Fig. 4b) of samples was measured by the Vernier caliper with an accuracy of 0.01 mm. The larger the worn length *d*, the larger the volume loss of the sample, so the worse of wear resistance of the sample.

### 3 Results and Discussion

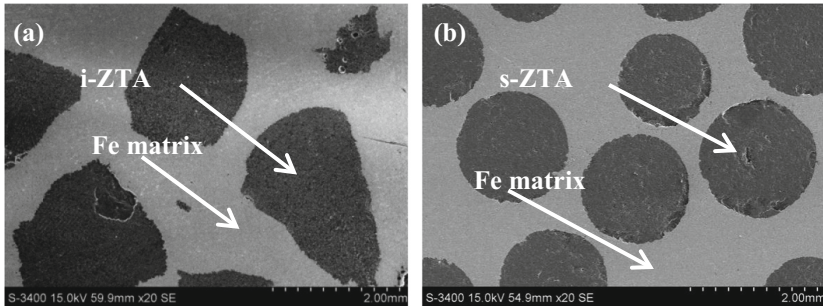
#### 3.1 Microstructure and Properties

Figure 5 shows XRD analysis result of the ZTA reinforced iron matrix composites. The phase constituents of ZTA reinforced iron matrix composites consists of Fe-Cr-Ni, (Fe, Cr)<sub>7</sub>C<sub>3</sub>, FeCrB of the Fe45 matrix, Al<sub>2</sub>O<sub>3</sub> and ZrO<sub>2</sub>.



**Fig. 5.** XRD analysis result of the ZTA reinforced iron matrix composites

Figure 6 shows the microstructure of composites reinforced by different shape ZTAp. It can be seen that the ZTAp is homogeneously distributed in Fe45 matrix and the interface between the ZTA particles and iron matrix looks better, which indicates the better wetness between the half-molten iron matrix and the ZTA particles during the sintering progress.



**Fig. 6.** Microstructure of iron matrix composites reinforced with (a) i-ZTAp and (b) s-ZTAp

Figure 7 shows the EDS line scan crossing ZTA particle and iron matrix, which is from the ZTA particle zone to iron matrix zone. From individual element distribution curve, it is obvious that the elements both in the ZTA particles and in the iron matrix haven't inter-diffused during sintering, which indicates that the interface between ZTAp and iron matrix is in the form of non-chemical bonding.

The densities of the composites with different particle size and content measured by drainage method are shown in Fig. 8. The density of sintered Fe45 matrix sample is  $7.53 \text{ g/cm}^3$ , close to its theoretical density of  $7.56 \text{ g/cm}^3$ . The density of i-ZTA particles and s-ZTA particles is  $4.58 \text{ g/cm}^3$  and  $3.10 \text{ g/cm}^3$  respectively. Because the density of ZTAp is lower than that of Fe45 self-fluxing alloy, the overall density of the composites decreases as the volume fraction of ZTAp increases. According to the rule

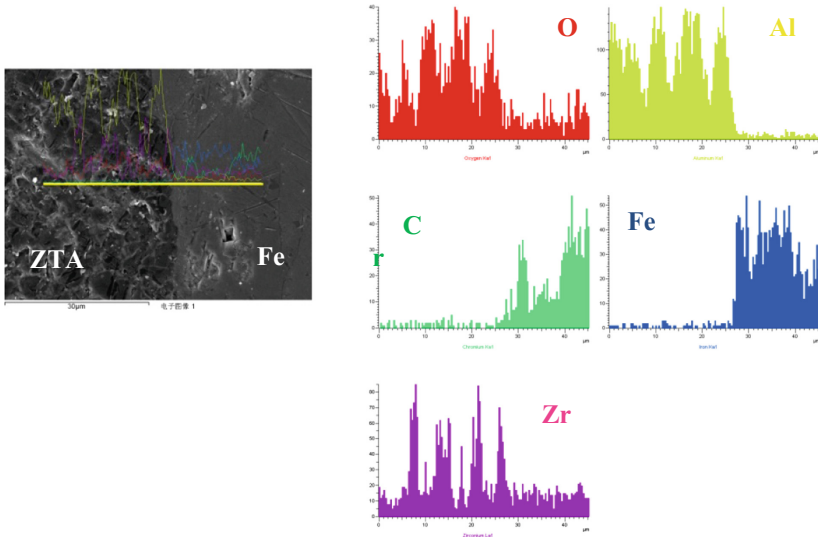


**Fig. 7.** Result of EDS line scan of ZTAp reinforced iron matrix composites

of mixture, the higher the volume fraction of ZTA particles is, the lower the density of composites is. When volume fraction of ZTAp is same, the density of the composite drops with the ZTA particle size decreases. That is because the smaller the particle size, the larger the surface area of the ZTAp, which results in the increase in the probability of the pores in the contact area as well as the decrease of the composite density. Because the density of i-ZTA particles is higher than that of s-ZTA particles, the density of i-ZTA particles reinforced iron matrix composites is higher than that of s-ZTA particles reinforced iron matrix composites under the same conditions.

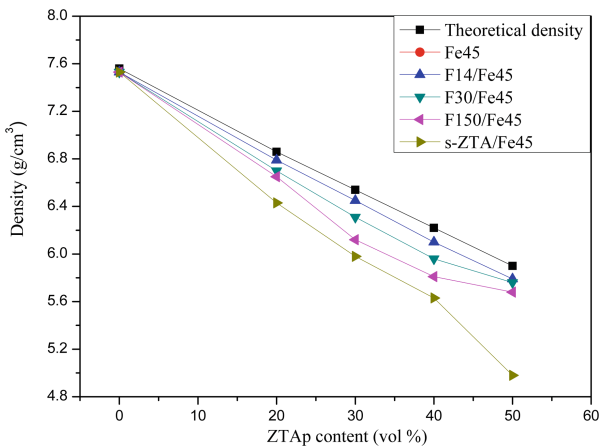


**Fig. 8.** Densities of the composites

Figure 9 shows the matrix hardness of the composites. It is clear that the matrix hardness is related to the content and size of particles. For 2 mm particles (F14 and s-ZTA), the hardness increases with the particle content when it is lower than 40 vol. %. That is because the addition of ZTA results in the lattice distortion of the matrix, which causes strain hardening. However, when the particle content reaches 50 vol. %, ZTA particles can cause the porosity of the composite, and hence result in decreases the matrix hardness of the composites. The smaller size particles are easier to result in the porosity of the composites, therefore the hardness of F30/Fe45 decreases at 40 vol. % content, even the hardness of F150/Fe45 drops obviously.

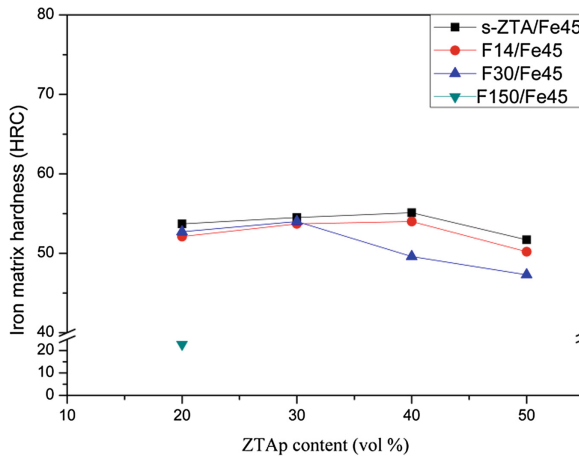


Fig. 9. Hardness of the composites

As mentioned above, the higher hardness is obtained when the iron matrix is reinforced by 20–40 vol. % ZTA with the particle size about 2 mm (F14 and s-ZTA).

### 3.2 Sliding Wear

The sliding wear test results of the composites are shown in Fig. 10. It is clearly seen that in spite of the differences of ZTA particle shape and size, the composites with 20 vol. % and 30 vol. % ZTA present lower wear volume than Fe45 matrix. Therefore, they have better wear resistance than Fe45 matrix, and composites with 30 vol. % ZTA show the best wear resistance. However, when ZTA content reaches 50%, the composites display worse wear resistance than Fe45 matrix. F30/Fe45 composite with 40% vol. smaller size ZTA show the similar behavior. Consequently, higher hardness and density will enhance the wear resistance of the composites.

Figure 11 is the morphology of worn Fe45 matrix specimen. From low magnification morphology Fig. 11(a) light gray strip deformation can be seen besides some plowing. As shown at high magnification Fig. 11(b), the light strip presents severe



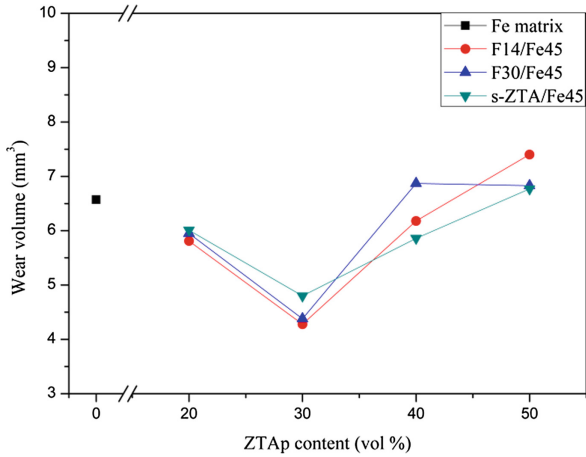


Fig. 10. Wear volume of composites

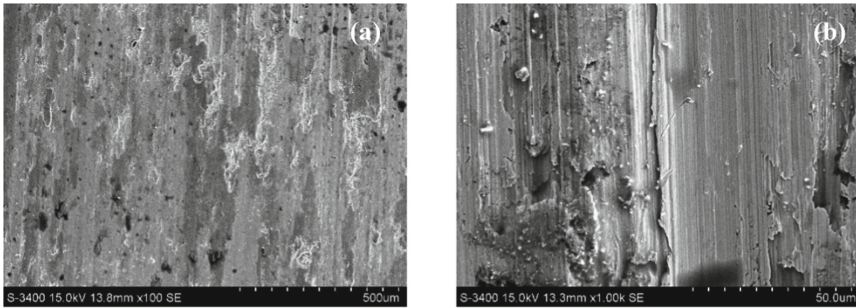


Fig. 11. Worn morphology of Fe45 matrix (a) low magnification and (b) high magnification

plastic deformation and thin plowing. Therefore, the wear mechanisms of the Fe45 matrix are that Al<sub>2</sub>O<sub>3</sub> wheel gives rise to severe plastic deformation and micro-plowing or micro-cutting.

Figure 12(a) and (b) are the worn morphology of the composite reinforced with F14 and F30 i-ZTA particles respectively. There are noticeable plows on the Fe matrix and the plows stop when they meet with ZTAp, which manifests that the ZTAp plays an obstacle role to plowing.

Worn morphologies of the composites reinforced by different ZTAp contents under sliding wear condition are shown in Fig. 13. It represents worn morphology of F14/Fe45 composites with 30 vol. % as Fig. 13(a) and 50 vol. % ZTAp as Fig. 13(b), respectively. It can be obviously seen that when the particle size is the same, the composite with 50 vol. % ZTAp presents poor bonding between the ZTAp and the matrix. Therefore, the ZTA particles are easy to be pulled out under the action of harder

asperities of  $\text{Al}_2\text{O}_3$  wheel and lose their hinder role. That is the reason why wear resistance of the composite with 50 vol. % ZTAp is worse than the iron matrix material without ZTAp.

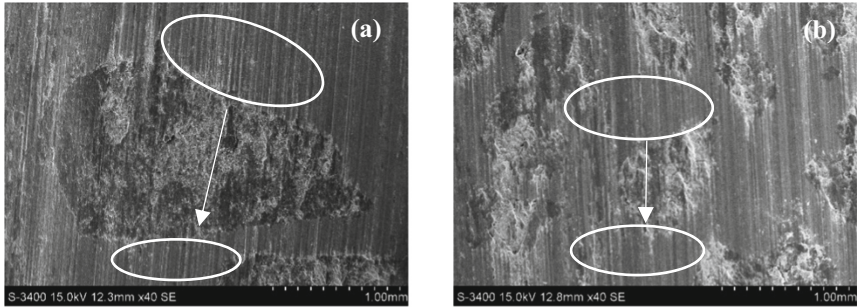


**Fig. 12.** Worn morphology of composites (a) F14/Fe45 and (b) F30/Fe45

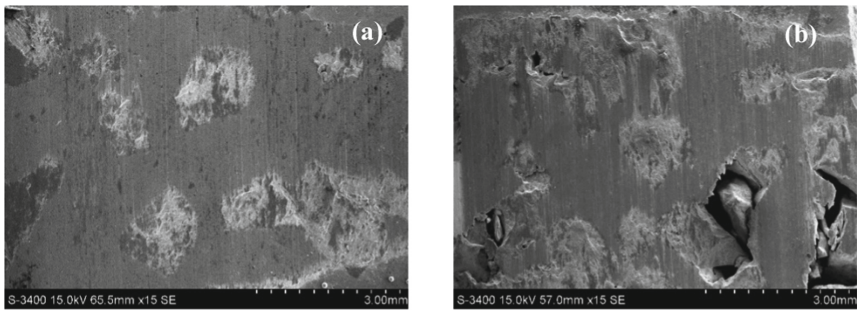


**Fig. 13.** Worn morphology of composites (a) 30 vol. % F14/Fe45, (b) 50% vol. % F14/Fe45

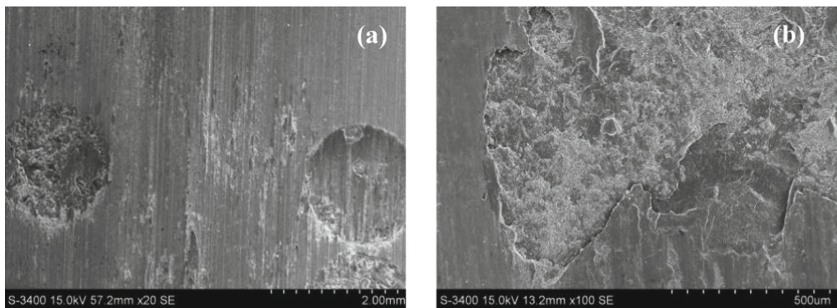


**Fig. 14.** Worn morphology of composites (a) s-ZTAp/Fe45, (b) s-ZTAp

Figure 14 is the worn morphology of the s-ZTA reinforced iron matrix composite. Compared to Fig. 13, we can find that the s-ZTAp is easy to be worn out. The reason is that the hardness of s-ZTAp (960 HV) is lower than that of  $\text{Al}_2\text{O}_3$  (1600HV) and i-ZTAp (1400 HV). The microstructure of s-ZTA is not as dense as i-ZTAp.

### 3.3 Three-Body Abrasive Wear Resistance

The worn zone lengths of the three specimens are shown in Fig. 15. It can be found that the worn zone lengths of iron matrix composite reinforced by i-ZTA and s-ZTA were shorter than iron matrix without reinforced particles. According to Richardson's theory [20], the wear rate decreases sharply when material hardness ( $H_m$ ) and abrasive hardness ( $H_a$ ) are with the ratio  $H_m/H_a \geq 0.8$ , and the wear resistance of the material will be significantly improved. In this paper, the same matrix material was adopted, and the hardness of the s-ZTA (960HV) and i-ZTA (1400HV) particles was near or higher than the abrasive hardness (quartz sand, HV1150). Therefore, the iron matrix composite reinforced by ZTA particles performs better wear resistance than that of iron matrix. This was mainly instigated by the combination of the supportive effect of iron matrix on ZTA particles and the protective effect of ZTAp on iron matrix in the composites.

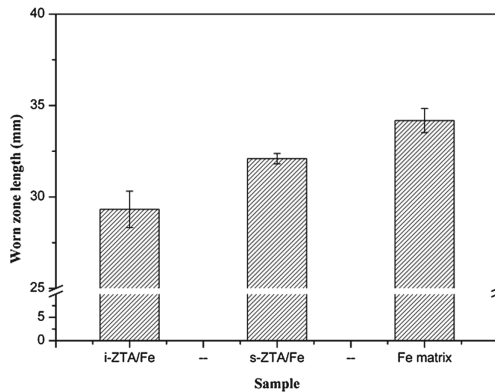
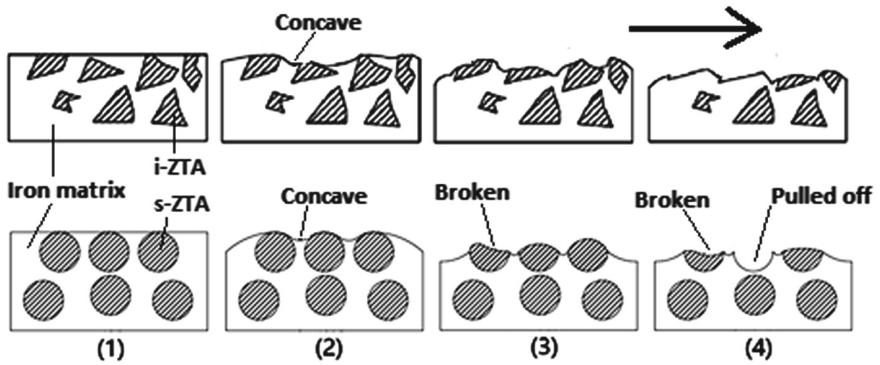


Fig. 15. Worn zone length of samples after three-body abrasive wear

The physical models of the three-body abrasive wear for the different shape ZTA particle reinforced iron matrix composite are shown in Fig. 16. Before the wear test, the ZTA particles and the iron matrix are in the same plane (Fig. 16(1)). At the first period of the wear test, the wear loss of the composite is large, and mainly triggered by the losses of the iron matrix (Fig. 16(2)). For the low hardness, the iron matrix is worn off mainly as the form of micro ploughing and micro cutting by the abrasives (Fig. 17).

With the increase of wear time, the iron matrix of the composite is worn to concave due to its low hardness (Figs. 16(2, 3) and 18). Therefore, the ZTA particles protrude out of the iron matrix, bear the main wear force of the abrasive (quartz sand), and have a protective effect on around iron matrix. Meanwhile, the concaved iron matrix has also



**Fig. 16.** Physical model of the three-body abrasive wear mechanism of composite: (1) before wear test; (2) first, (3) second, and (4) third period of the wear test. The arrow represents the direction of abrasive movement.

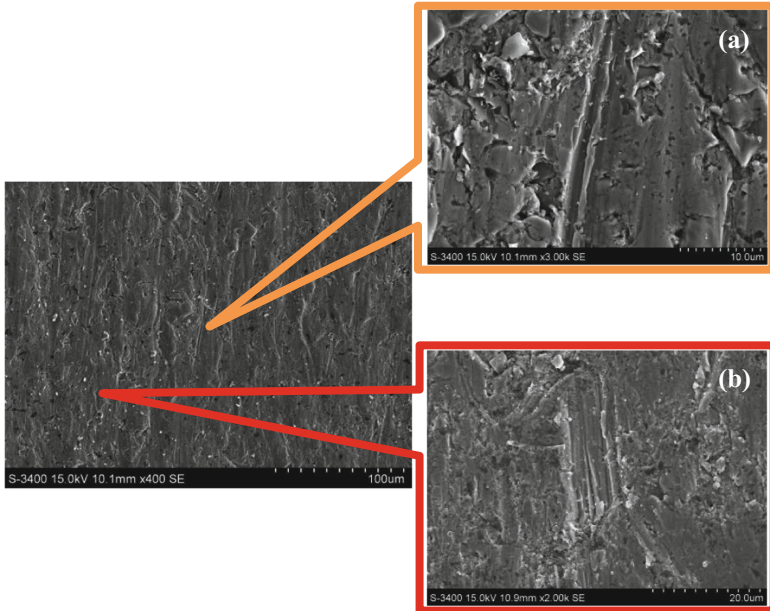


**Fig. 17.** SEM images of iron matrix after the wear test: (a) micro-ploughing; (b) micro-cutting.

a supportive effect on the ZTA particles [9]. Thus, the supportive effect of the iron matrix on ZTA particles and the protective effect of ZTA particles on the iron matrix play a combined role. So the wear losses of the composite decrease gradually until the wear state was reached at the third period of the test. At the third period of the wear test (Fig. 16(4)), the iron matrix of the composite was worn to concave so severely that the supportive effect of the matrix on ZTA particles became deficient, thus, it was found

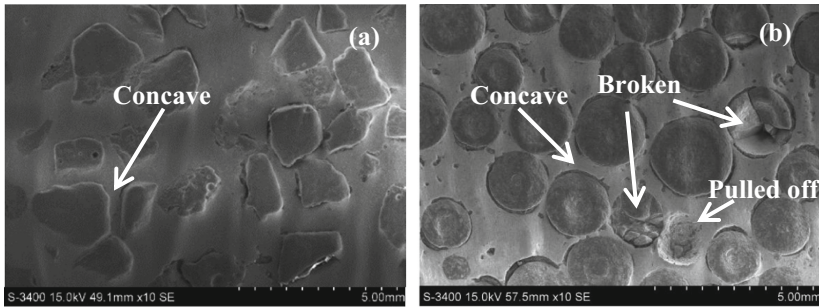


**Fig. 18.** SEM images of the composite after three-body abrasive wear (a) Reinforced by i-ZTA; (b) reinforced by s-ZTA.

some ZTA particles were broken, or even pulled off (Fig. 18). As a result, the wear volume loss of the composite was increased.

From Figs. 15 and 18, we can see that the composite reinforced by i-ZTA perform better wear resistance than that reinforced by s-ZTA. Because of multi-angle geometric shape of i-ZTA particles, they can be wrapped more tightly by the iron matrix than the s-ZTA for the non-chemical bonding. i-ZTA was more difficult to be pulled off from iron matrix during the friction and wear progress, so the wear resistance of the composite reinforced by i-ZTA particles performs better. Furthermore, higher hardness and dense microstructure of i-ZTA are also the reasons why that the wear resistance of i-ZTA reinforced iron matrix composites is better than that of s-ZTA.

## 4 Conclusions

1. ZTA particles can be uniformly distributed in iron matrix by powder metallurgy. The interface between ZTA and iron matrix shows the evidence of non-chemical bonding.
2. The composite with 30 vol. % ZTA exhibits the best wear resistance during sliding wear.
3. The supportive effect of the iron matrix on ZTA and the protective effect of ZTA on the iron matrix of the composite improve wear resistance of the composites during the three-body abrasive process.
4. Comparing to s-ZTA, i-ZTA has higher hardness, density, as well as multi-angle shape, so i-ZTA reinforced iron matrix composite shows better wear resistance for i-ZTA is not easy to be pulled off from the iron matrix.

## References

1. Tirosh, J., Shachak, N., Shirizly, A., et al.: Thermal-history effect on the yield strength of particulate metal matrix composite. *Int. J. Mech. Sci.* **78**(1), 52–59 (2014)
2. Zhou, R., Jiang, Y., Lu, D.: The effect of volume fraction of WC particles on erosion resistance of WC reinforced iron matrix surface composites. *Wear* **255**(1–6), 134–138 (2003)
3. Premnath, A.A., Alwarsamy, T., Rajmohan, T., et al.: The influence of alumina on mechanical and tribological characteristics of graphite particle reinforced hybrid Al-MMC. *J. Mech. Sci. Technol.* **28**(11), 4737–4744 (2014)
4. Fedrizzi, A., Pellizzari, M., Zadra, M.: Production of a particle reinforced hot work tool steel by mechanical alloying. *La Metall. Ital.* **105**(3), 39–46 (2013)
5. Cesari, F., Esposito, L., Furgiuele, F.M., Maletta, C., Tucci, A.: Fracture toughness of alumina-zirconia composites. *Ceram. Int.* **32**(3), 249–255 (2006)
6. Maiti, K., Sil, A.: Microstructural relationship with fracture toughness of un-doped and rare earths (Y, La) doped  $\text{Al}_2\text{O}_3\text{-ZrO}_2$  ceramic composites. *Ceram. Int.* **37**(7), 2411–2421 (2011)
7. Tsukuma, K., Ueda, K., Shimda, M.: Strength and fracture toughness of hot isostatic-pressed  $\text{Y}_2\text{O}_3$ -partially stabilized  $\text{ZrO}_2/\text{Al}_2\text{O}_3$  composites. *J. Am. Ceram. Soc.* **68**(1), C-4–C-5 (2006)
8. Srdic, V.V., Radonjic, L.: Transformation toughening in sol-gel derived alumina-zirconia composites. *J. Am. Ceram. Soc.* **80**(8), 2056–2060 (1997)
9. Li, Z.L., Jiang, Y.H., Zhou, R., Lu, D., Zhou, R.: Dry three-body abrasive wear behavior of WC reinforced iron matrix surface composites produced by V-EPC infiltration casting process. *Wear* **262**(5–6), 649–654 (2007)
10. Rezaei, M.R., Shabestari, S.G., Razavi, S.H.: Effect of ECAP consolidation temperature on the microstructure and mechanical properties of Al-Cu-Ti metallic glass reinforced aluminum matrix composite. *J. Mater. Sci. Technol.* **33**(09), 1031–1038 (2017)
11. Shi, H.L., Wang, X.J., Zhang, C.L., Li, C.D., Ding, C., Wu, K., Hu, X.S.: A novel melt processing for Mg matrix composites reinforced by multiwalled carbon nanotubes. *J. Mater. Sci. Technol.* **32**(12), 1303–1308 (2016)
12. Skolianos, S., Kattamis, T.Z., Chen, M., Chambers, B.V.: Cast microstructure and tribological properties of particulate TiC-reinforced Ni-base or stainless steel matrix composites. *Mater. Sci. Eng., A* **183**(1–2), 195–204 (1994)
13. Wanjara, P., Drew, R.A.L., Root, J., Yue, S.: Evidence for stable stoichiometric Ti<sub>2</sub>C at the interface in TiC particulate reinforced Ti alloy composites. *Acta Mater.* **48**(7), 1443–1450 (2000)
14. Wang, Y., Wang, H.Y., Yang, Y.F., Jiang, Q.C.: Solidification behavior of cast TiB<sub>2</sub> particulate reinforced Mg composites. *Mater. Sci. Eng. A* **478**(1–2), 9–15 (2008)
15. Karimzadeh, F., Enayati, M.H., Tavooosi, M.: Synthesis and characterization of Zn/Al<sub>2</sub>O<sub>3</sub> nanocomposite by mechanical alloying. *Mater. Sci. Eng. A* **486**(1–2), 45–48 (2008)
16. Song, T.F., Jiang, X.S., Shao, Z.Y., Mo, D.F., et al.: Interfacial microstructure and mechanical properties of diffusion-bonded joints of titanium TC4 (Ti-6Al-4 V) and Kovar (Fe-29Ni-17Co) alloys. *J. Iron Steel Res. (Int.)* **24**(10), 1023–1031 (2017)
17. Varol, T., Canakci, A., Ozsahin, S.: Modeling of the prediction of densification behavior of powder metallurgy Al-Cu-Mg/B<sub>4</sub>C composites using artificial neural networks. *Acta Metall. Sinica (Engl. Lett.)* **28**(02), 182–195 (2015)

18. Mahesh, K., Sankaran, S., Venugopal, P.: Microstructural characterization and mechanical properties of powder metallurgy dual phase steel preforms. *J. Mater. Sci. Technol.* **28**(12), 1085–1094 (2012)
19. Ravichandran, M., Naveensait, A., Anandakrishnan, V.: Al-TiO<sub>2</sub>-Gr powder metallurgy hybrid composites with cold upset forging. *Rare Met.* **6**, 686–696 (2014)
20. Richardson, R.C.D.: The wear of metals by hard abrasives. *Wear* **10**(4), 291–309 (1967)